Available online at www.sciencedirect.com

ScienceDirect

Physics Procedia 56 (2014) 835 – 844

Physics Procedia

8th International Conference on Photonic Technologies LANE 2014

A combined experimental and numerical approach to the laser joining of hybrid Polymer – Metal parts

E. Rodríguez-Vidal[a,]*, J, Lambarri[a], C. Soriano[a], C. Sanz[a], G. Verhaeghe[b]

[a]*IK4-Tekniker, Advanced Manufacturing Technologies Unit, Iñaki Goenaga 5, 20600 - Eibar (Gipuzkoa), Spain*
[b]*Faurecia Autositze GmbH, Nordsehler Strasse 38,Stadthagen, 31655, Germany*

Abstract

A two-step method for the joining of opaque polymer to metal is presented. Firstly, the metal is structured locally on a micro-scale level, to ensure adhesion with the polymeric counterpart. In a second step, the opposite side of the micro-structured metal is irradiated by means of a laser source. The heat thereby created is conducted by the metal and results in the melting of the polymer at the interface. The polymer thereby adheres to the metal and flows into the previously engraved structures, creating an additional mechanical interlock between the two materials. The welding parameters are fine-tuned with the assistance of a finite element model, to ensure the required interface temperature. The method is illustrated using a dual phase steel joined to a fiber-reinforced polyamide. The effect of different microstructures, in particular geometry and cavity aspect ratio, on the joint's tensile-shear mechanical performance is discussed.

Peer-review under responsibility of the Bayerisches Laserzentrum GmbH

Keywords: polymer-metal hybrid joints; laser joining; laser structuring; glass fiber reinforced

1. Introduction

The search for lightweight and low-cost structures and therefore, reduced energy consumption and greenhouse gas emissions, particularly CO_2, is pushing the transportation industry towards the introduction of multi – material designs, which include components made of metals, polymers and/or composites. Non – metallic materials are

* Corresponding author. Tel.: +34-943-206-744 ; fax: +34-943-202-744 .
E-mail address: eva.rodriguez@tekniker.es

Peer-review under responsibility of the Bayerisches Laserzentrum GmbH
doi:10.1016/j.phpro.2014.08.101

attractive because they exhibit low weight, high corrosion resistance, ease of processing and recycling, excellent formability and great design flexibility. In this way, hybrid assemblies combine the best of the two worlds, mechanical performance at a reduced weight. However, since presently metals cannot be excluded altogether from structural parts, the introduction of new manufacturing processes, and particularly union technologies able to provide high quality joints, with repeatability and at the required productivity rates, is becoming increasingly important. Currently, industrially accepted joining methods can be classified into two categories, Post Molding Assembly (PMA) and In Molding Assembly (IMA), Paul et al. (2012). PMA can be further divided into adhesive bonding and mechanical joining (screws, rivets, bolts, etc). Adhesive bonding is based on the introduction of a chemical adhesive at the plastic – metal interface. It's a relatively simple process, but non – environmentally friendly and it requires extensive preparation, long curing times and can suffer from deterioration by external influences and low mechanical resistance. Mechanical joining also requires careful preparation and additional drawbacks are the need for extra assembly elements and poor flexibility in joint design. On the other hand, IMA doesn't require any extra steps, although the joint design possibilities are limited. In Gruijic et al. (2008) a number of different approaches for polymer metal hybrid joining are reviewed, and the conclusion is that the one based on micro-scale mechanical interlocking is the most promising, in terms of metal surface preparation requirements, compatibility with the injection molding process and durability of polymer – metal bond.

An alternative technology for the generation of sound hybrid joints is the direct thermal laser joining of plastic and metal. Depending on the polymer optical properties at the source wavelength, two variants exist. In laser transmission joining, the polymer is transparent to the laser radiation to a high degree. Therefore, it is possible to reach the interface through the polymer. By contrast, in conduction joining, the polymer is opaque to the laser wavelength, so the metal is radiated directly, and the heat transported by conduction to the interface.

The laser joining approach was first demonstrated at the Joining and Welding Research Institute of Osaka University by Kawahito et al. (2006) and Katayama et al. (2007). In these pioneering works, unions of stainless steel to polyethylene terephthalate (PET), polyamide (PA), polycarbonate (PC) and polypropylene (PP) were generated. Parts with high shear strength were found, and it was suggested that it was due to the possibility of both chemical and physical bonding. Since then, the technique has been extended to various material combinations, such as DC01 steel to PA6.6, Bergmann and Stambke (2012), aluminum to PC, PA and glass fiber reinforced polyamide, Amend et al. (2013), 304 stainless steel to PMMA, Hussein et al. (2013) and zinc – coated steel to carbon fiber reinforced polyamide, Jung et al. (2013).

A way to further enhance the hybrid joint performance is to generate a micro pattern on the metal surface, so as to provide an extra mechanical interlock. Besides process parameters for the joining operation, such as laser power, speed or applied clamping pressure, the nature and geometrical features of the engraved patterns have been proven to be key parameters for the mechanical performance of polymer – metal hybrid unions, as was demonstrated in Roesner et al. (2011), Bergmann and Stambke (2012) and Cenigaonaindia et al. (2012).

Besides the generation of lightweight structures for the transportation industry, potential applications can also be found in the biomedical sector, for MEMs and BioMEMs devices, as shown in Georgiev et al. (2009), where pure titanium and Teflon joints were proven to be feasible, and in Wang et al. (2010) where titanium and PET foil unions were successfully generated. Both of these works are based on transmission welding with no micro –structuring, and the resulting strength is mainly attributed to the formation of chemical bonds, such as Ti – F or Ti – C.

In the present work, a two – step method for the joining of opaque polymers to metals is presented. Both the micro – structuring and the joining operation are conducted by a laser source. A finite element model is used to assist in the parameter selection for the joining operation. The method is then illustrated using a dual phase steel joined to a fiber-reinforced polyamide, and the effect of different microstructures, in particular geometry and cavity aspect ratio, on the joint's tensile – shear mechanical performance is discussed.

2. Experimental procedure

The materials employed in this work were a dual phase steel (DP1000) and glass reinforced polyamide (PA6 -GF30). Sample dimensions were 80x25x1 mm^3 and 80x25x4 mm^3 for metal and polyamide respectively.

Initially, metal specimens were laser – structured by a 200 W CW and a 40 W ns fiber laser sources, in order to study the influence of the structuring geometry on the behavior of the adhesion force between the joining partners.

A total surface of 15x20 mm^2 was structured on the metal samples by means of single parallel grooves oriented perpendicularly to the long edge of the plates. Different tests were done, for both lasers, rescanning the surface a different number of times, N_i *(i=1, 2, 3)*, using the same patterns and processing parameters. Moreover, structure density values of 0.038 and 0.133 were fixed for CW and ns laser source respectively. Structure density is defined as the ratio of the structured area to the overall examined area, as stated by Roesner et al. (2011). In addition, the distance between consecutive grooves was fixed at 400 µm.

The effects of metal micro – structuring were examined by topographic analysis. First, top views were extracted via optical microscopy in order to determine the surface quality of the grooves. Then, cross sections of the specimens were mounted into an Epoxy resin, to analyze the depth and aspect ratio of the engraved structures.

The lap – joint configuration for the subsequent conductive joining process is shown in Fig. 1. The top material (i.e. metal) overlaps 20 mm with the bottom material (i.e. polyamide), so that the overall length of the joint sample is about 140 mm. The CW laser source was employed for the joining process with a defocused 1 mm diameter spot. This spot was swept at high frequency for 10 mm, parallel to the long edge of the plate, using a galvo scanning system, in order to generate an effective rectangular spot of 1x10 mm^2. The latter was then displaced at 360 mm/min, in the same direction in which the grooves were produced, over the metal surface so as to produce a total joint area of 10x20 mm^2, as shown by the shaded surface on the top view of Fig. 1. The joining parameters were kept constant with the aim to study the influence of the structure pattern on the joint quality. Both materials were clamped by applying a uniform pressure with a pneumatic clamping device, in order to enhance the flow of the molten plastic material into the microstructures of the steel.

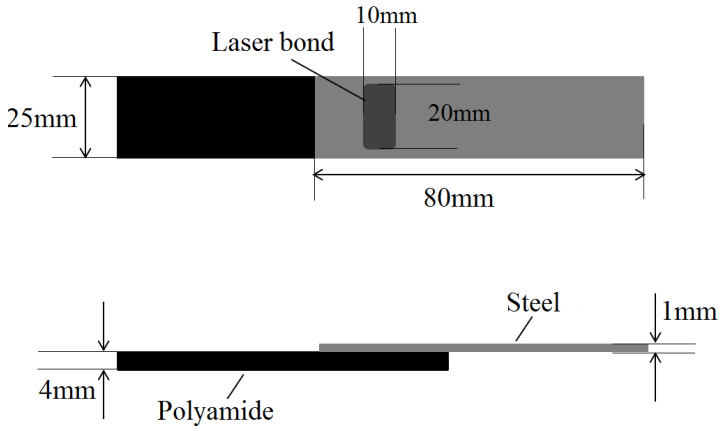

Fig. 1. Schematic lap – joint configuration.

The mechanical performance of the joints was investigated by tensile shear tests to measure the joint strength, using a testing machine with a maximum load capacity of 50 kN and a cross – head displacement rate of 5 mm/min. For each experimental condition, five specimens were tested to ensure the reproducibility of the results.

3. FEM thermal model of the joining process

In order for the joining process to be successful, one necessary condition is that the interface temperature, on the polymer side, must lie within a predefined range, Holtkamp et al. (2010). The limits of this interval are given, on the lower boundary, by the melting point of the polymer while the upper boundary is given by the degradation onset temperature. However, experimentally, the joint temperature is not directly measurable. Therefore, to avoid a costly and time consuming trial and error approach, a finite element (FEM) model of the thermal aspects of the joining process has been developed. The main goal of the model is to predict the process parameter window that ensures an appropriate interface temperature, for the considered laser source and material combination. Another advantage of the model is the possibility to relate the temperature on the irradiated metallic surface, which can be monitored experimentally by the use of non-contact methods, with the joint temperature. In this way, control strategies can be studied, in order to avoid undesirable effects such as lack of fusion or overheating, which can appear when working with open – loop approaches.

The heat equation has been solved using the commercial software package Comsol Multiphysics, in a geometry corresponding to the real test parts in lap – joint configuration, as the one shown in Fig. 1.

$$\rho C_p \frac{\partial T}{\partial t} = \nabla \cdot (\kappa \nabla T) + Q \tag{1}$$

In Eq. 1, ρ represents density, C_p the specific heat and κ the thermal conductivity of the materials. Q is a volumetric heat source, and in this case $Q = 0$, since the energy input is introduced as a boundary heat source and latent heats are disregarded. Further details on thermophysical properties can be found in section 2.2.3. The general form of the boundary conditions is given by Eq. (2):

$$-n\left(-\kappa \nabla T\right) = q + h\left(T_{ext} - T\right) + \sigma\varepsilon\left(T^4{}_{ext} - T^4\right) \tag{2}$$

In Eq. 2, q represents a boundary heat source, h the heat transfer coefficient, σ the Steffan – Boltzmann constant and ε the emissivity of the material. Given the configuration of the clamping tool, only a section of the metal surface is exposed to the atmosphere, the one shown as a shaded region in the top view of the geometry in Fig. 1. This surface is the one subjected to the laser radiation, so $q = 0$ for any boundary other than this. The details of the heat source implementation can be found in section 2.2.1. Similarly, for this open boundary the heat transfer coefficient is set to a standard value for a free convection on air, h_0. The rest of the surfaces are in direct contact with the clamping system, and this is modeled by an artificially high heat transfer coefficient, $h_1 >> h_0$. Regarding the emissivity, it is considered to be different from zero only in the upper exposed surface. The surfaces pertaining to the metal – polymer interface have a special status, since the thermal resistance of the joint has been considered, as is explained in section 2.2.2.

3.1.1. Heat source description and energy coupling

The heat input into the model is considered as a boundary heat source, q in Eq. 2, acting on the metal top surface, but only on the shaded region shown in the top view of Fig. 1. The actual laser spot, at the working distance, is a defocused 1 mm diameter source, with Gaussian – like power density distribution. This source describes a 10 mm linear movement at high speed, $v_x = 3$ m/s, and the whole 10x20 mm^2 surface is covered by overlapping such individual lines. In the present case, in order to simplify the model, an effective spot is considered, which is the result of integrating the power density of the Gaussian – like source along a single line, and then diving this result by the time it takes to travel such line, so as to recover proper power density units. Considering the time it takes to sweep a single line, and the idle time in between lines, the speed v_y of the effective spot, φ_{eff} can be obtained. φ_{eff} is found by numerical integration on a 2D domain, in the framework of the same software.

The efficiency of the laser – metal coupling is a key element for the model accuracy. This is determined by the absorption coefficient, which is in general a complex function of the material (real and imaginary parts of the refractive index), radiation properties (wavelength, polarization state), angle of incidence and surface characteristics (roughness, presence of defects, oxide layers). Since some of these magnitudes are also temperature dependent, an *a priori* determination of the absorption coefficient, based purely on theoretical grounds, is a complex task. In this work an alternative empirical approach is proposed, based on the following steps:

1. The spectral reflectance of the as – received metallic sample is obtained at room temperature, using a spectrophotometer and an integrating sphere. Then the corresponding value at the laser wavelength, 1070 nm, is extracted and the absorbance inferred from the energy balance, assuming zero transmittance.
2. A small number of experimental tests are carried out at different process parameters. In this way, different temperatures are induced at the lower metal surface, which are recorded experimentally using thermal labels. The model is evaluated with the absorption coefficient as a running parameter, until both numerical and experimental values agree for each case. Then, the corresponding absorption value is associated with the steady state maximum upper surface temperature.
3. Finally the curve $A = A(T)$ is constructed, which determines the dependence of the absorption coefficient on temperature.

Combining the effective power density and the expression for the temperature dependent absorbance, the final expression for the boundary heat source is obtained:

$$q = A(T)\varphi_{eff}(x, y, t) \tag{3}$$

3.1.2. Thermal contact sub model

In order to have a more accurate prediction of the metal – polymer interface temperature, the thermal contact resistance (TCR) of the union is considered. This implies that the metal and polymer sides of the interface exhibit different temperatures during the thermal cycle. In principle, there are three different heat transfer mechanisms for two conforming surfaces in contact: conduction through the discrete contact spots, energy transfer through the gas trapped between the layers and heat transfer due to radiation. However, radiation in the voids can be considered negligible if the temperatures are smaller than 1000 ºC, as stated by Fenech and Rohsenow (1963). Since in this case the previously stated condition holds, the following expression for the TCR coefficient is adopted:

$$h = h_c + h_g \tag{4}$$

In Eq. 4, h_c represents the constriction conductance and h_g is the gas gap conductance. In this case a Cooper – Mikic – Yovanovich relation is assumed for h_c:

$$h_c = 1.25\kappa_{contact}\frac{m_{asp}}{\sigma_{asp}}\left(\frac{p}{H_c}\right)^{0.95} \tag{5}$$

Where $\kappa_{contact}$ is the harmonic mean of the thermal conductivities, m_{asp} is the combined absolute average asperity slope, σ_{asp} is the combined RMS roughness, p is the applied pressure and H_c is the microhardness of the softer material, in this case the polymer. The values for m_{asp} and σ_{asp} were calculated from experimentally obtained 1D profiles of the mating surfaces. H_c was also measured experimentally, by a microhardness tester, while the applied pressure is known from the clamping system readout.

The expression for the gas gap conductance is:

$$h_g = \frac{\kappa_{gap}}{Y + M} \tag{6}$$

In Eq. 6, κ_{gap} is the thermal conductivity of the interstitial fluid, in this case air, Y is the separation distance between the mean planes of the conducting surfaces and M is the gas parameter. Details on how to evaluate these magnitudes can be found in Yüncü (2006).

3.1.3. Thermophysical properties

Thermophysical properties, in particular density, thermal conductivity and specific heat are also important for quantitative predictions. For the dual phase steel, temperature dependent properties have been taken from literature, Schenk et al. (2009). For the polymeric counterpart, experimental tests have been carried out to evaluate critical temperatures (glass transition, degradation and melting) and the specific heat as a function of temperature. Degradation onset was determined by thermogravimetric analysis (TGA). A temperature range of 21-500 °C was studied, with a heating range of 20 °C/min under a nitrogen atmosphere. Melting point and glass transition were obtained by differential scanning calorimetry (DSC). Temperature range under study was -50-500 °C, also under a nitrogen atmosphere. Finally, specific heat was extracted also using DSC, by comparison with a sapphire sample of known properties, according to standard ASTM E 1269. Thermal conductivity and density were considered constant, and extracted from datasheets. For the fiber reinforced polyamide, the main results are summarized in the following table.

Table 1. Critical temperatures for the glass fiber reinforced polyamide.

Magnitude	Temperature (ºC)
Glass transition	49
Melting point	203
Degradation onset	394

4. Results and discussion

4.1. Laser structuring of steel

The results of the laser structuring of steel are shown in Fig. 2. Top views of the structured area (Fig. 2a, Fig. 2c) show clear differences in track width and amount of melt recast along the grooves. During the ns – processing, the material is uniformly ejected from the middle of the microstructure, as depicted in Fig. 2b. As it can be seen, groove depth and even height of the recast layer at the structure border are significantly raised when increasing the number of laser scans, N. On the other hand, the CW – structuring results reveal the presence of melt recasts along the grooves, as it can be observed in Fig. 2d. The latter entails a repetitive loss among the groove depths conducted with the same N. The main groove geometrical parameters obtained for both laser sources are summarized in Table 2, including the aspect ratio, which is obtained as the rate between depth and width of the micro-structures.

The results, obtained by analyzing the optical micrographs, reveal a meaningful difference in terms of aspect ratio between both geometries. CW – structuring shows deeper and narrower grooves than ns structures, but at the same time the standard deviation associated to the measured depth is greater than in the case of ns – structuring. Additionally, this standard deviation increases with the number of laser scans. This can be explained by the fact that bigger number of scans induces greater amount of melt recast along the grooves and thus, greater inhomogeneities. By contrast, ns – structuring shows a standard deviation associated to the measured depth independent of number of tracks, due to the fact that the material is ejected and the melt recast amount in minimal compared to CW – structuring. Furthermore, it is possible to observe that the ns micro – structure depth increases linearly with the

number of tracks while the behavior in case of CW – structuring seems to be different. The latter could be explained in terms of differences in dynamic behavior of the ejected and melt recast metal when the laser radiation is applied.

Table 2. Groove geometrical parameters.

Laser Source	Number of scans	Depth (µm)	Width (µm)	Aspect ratio
ns active fiber	2	19 ± 2	72 ± 2	0.26
ns active fiber	4	37 ± 2	72 ± 2	0.52
ns active fiber	6	56 ± 2	72 ± 2	0.78
CW active fiber	4	75 ± 32	21 ± 4	3.57
CW active fiber	8	133 ± 44	21 ± 4	6.33
CW active fiber	12	155 ± 56	21 ± 4	7.38

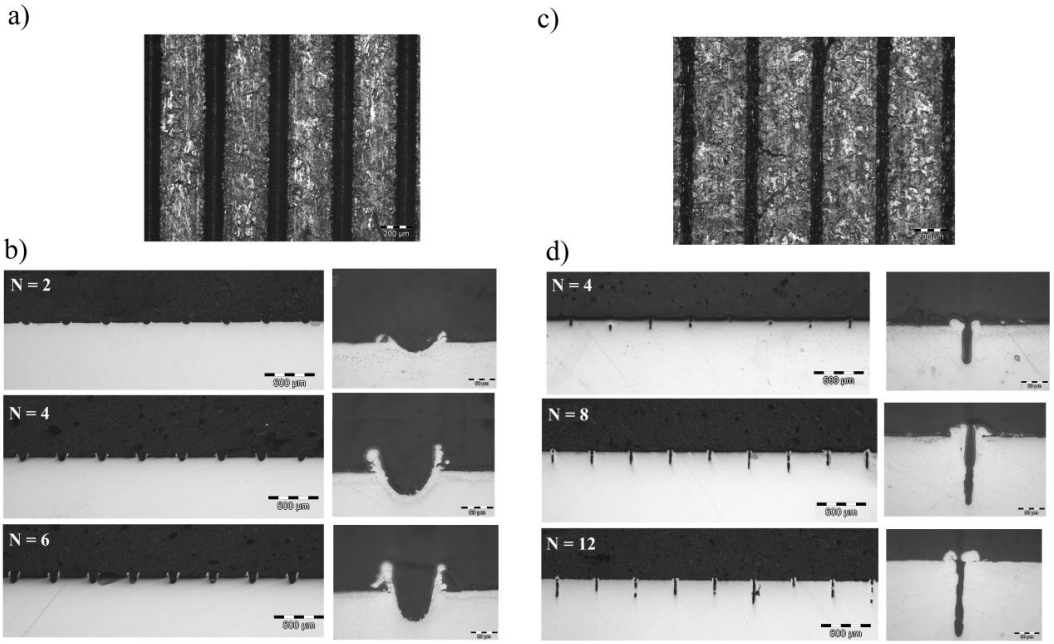

Fig. 2. Results of laser structuring of steel: (a) Top view of ns groove structures and (b) Cross-section of groove structures with different depths; (c) Top-view of CW groove structures and (d) Cross-section of CW groove structures with different depths.

4.2. FEM modeling of the joining process

The main result of the FEM model is the process parameter map shown in Fig. 3b. It divides the parameter space into different areas. The effective power density and effective interaction time are calculated assuming an effective spot, as defined in section 3.1.1. In Fig. 3a the maximum temperature reached at the polymer side of the interface is shown. The numerical map is then obtained by plotting the contours of this function, corresponding to the glass transition, melting point and degradation onset temperatures of the polymer, in the power density – interaction time parameter space.

The right process parameter combination can be found in between the melting point, at 203 ºC and the degradation onset temperature, 394 ºC. In order to provide maximum productivity, the highest available power

density, $2.2x10^7$ W/m^2, and an interaction time of 0.167s were employed experimentally. Using this same power density, an interaction time of 0.143s was also tested, but this combination didn´t provide polymer melting, as predicted by the model. Table 3 shows the error of the model when comparing the peak temperature measured at the metal side of the interface with the numerical prediction.

Additional information provided by the model includes thermal cycles, temperature gap at the interface, heating and cooling velocities and the depth and width of the molten area.

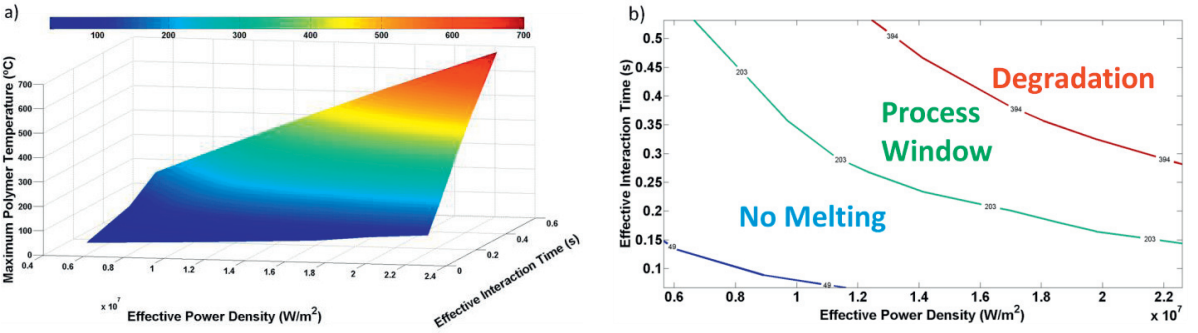

Fig. 3. (a) Highest temperature reached at the polymer side of the interface and (b) Process parameter map, dividing the parameter space into different regions.

Table 3. Numerical error for the peak temperature reached at the metal side of the interface.

Effective power density (W/m^2)	Effective interaction time (s)	Experimental temperature (ºC)	Predicted temperature (ºC)	Relative error
$2.2x10^7$	0.167	249	233	6.4%
$2.2x10^7$	0.143	218	197	9.6%
$2.2x10^7$	0.125	182	170	6.6%
$2.2x10^7$	0.1	<121°C	118	-

4.3. Conductive joining of polyamide to steel

The breaking force results of untreated and laser structured specimens are shown in Fig. 4, and the corresponding values are summarized in Table 4. For each pre-treatment, five specimens were tested, in order to have a good statistic. The bar graph in Fig. 4 shows the averaged breaking force along with the standard deviations for each micro-structuring condition.

All tested specimens experimented interface failure. For a non-structured sample, joining between both materials shows poor adhesion. It is worth to note a clear rise of breaking force when a pre-treatment of metal surface is considered.

According to Fig. 4, it is observed that breaking force of the joint increases, for both structure geometries, with increasing the number of scans. Particularly, breaking force values of the ns – structured specimens show a linear behavior. The resultant maximum breaking force for CW – structured samples, obtained for the considered number of tracks, evidence a lower quality joint than in the ns – structured case. As it can be seen in Table 4, the maximum breaking force achieved, $(F_{N=12})_{CW}=1834 \pm 297$ *N*, is comparable to the minimum value found for the ns – structured samples $(F_{N=2})_{ns}=1718\pm 203$*N*. Additionally, the joints corresponding to CW structures shown larger standard deviations (in %) than that observed in the case of joints performed with ns structures. This fact is in agreement with the standard deviation trend observed in the micro – structuring depths performed by the ns and CW fiber lasers (Table 4). Taking into account the aforesaid standard deviation associated to breaking force found in the case of CW

structuring, there is not a clear evidence of breaking force increases for greater number of rescans ($N_{tracks} > 8$). Also, the standard deviation associated to the breaking force of joints with ns generated micro – structures is independent of number of tracks, in the same way as the standard deviation associated to the ns – microstructure depths (Table 4). Thus, the results reveal a clear influence of the metal pretreatment on the characteristics of the joints.

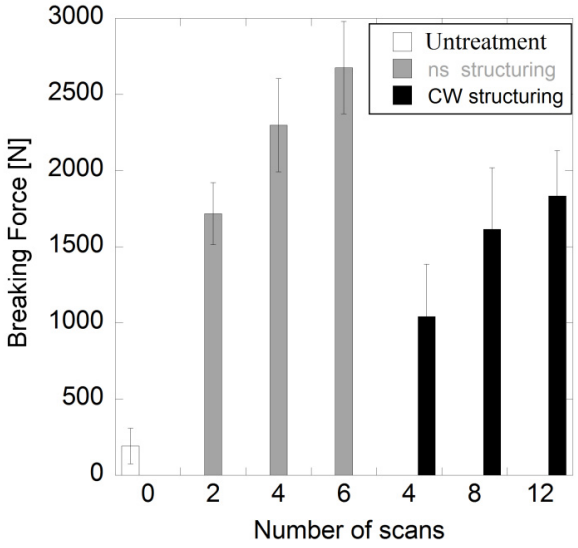

Fig. 4. Breaking force of PA6 - DP1000 joints, as a function of laser type and microstructure depth.

Table 4. Breaking force results considering the micro-structuring parameters listed in Table 2.

Laser Structuring Source	Laser Joining Source	Number of scans	Breaking Force [N]
Untreated	CW active fiber	0	191 ± 117
ns active fiber	CW active fiber	2	1718 ± 203
ns active fiber	CW active fiber	4	2298 ± 307
ns active fiber	CW active fiber	6	2676 ± 304
CW active fiber	CW active fiber	4	1043 ± 342
CW active fiber	CW active fiber	8	1615 ± 405
CW active fiber	CW active fiber	12	1834 ± 297

Further investigations are in progress to analyze the evolution of breaking force for higher values of ns micro – structure depths. Additionally, progress concerning the characterization of the specimens after tensile shear testing is needed, in order to provide better knowledge about the mechanisms responsible for interlocking. This, in turn, could shed some light on the meaningful difference on failure force values found for ns and CW micro – structures and the lack of a clear trend for the CW case.

5. Summary and conclusions

In this paper a novel combined experimental and numerical approach to laser joining of hybrid Polymer – Metal parts is reported. Experiments on conductive laser joining of glass reinforced polyamide to steel for different metal pretreatment conditions are performed. Two different structure geometries with three depths each are considered.

The conducted experiments show that the joining process cannot be successful without pretreatment. By contrast, strong joint connections of thermoplastic and metal are possible and can be produced by means of proper metal structuring.

The selection of parameters for the joining process is assisted by a FEM model, which is able to provide the parameter window for appropriate interface temperature with good accuracy, and thus, reduce notably the need for trial and error experiments.

Concerning the influence of metal pretreatment, the reported experiments demonstrate a clear influence of geometry and aspect ratio on the breaking force. In the case of ns micro – structures, the breaking force raises linearly when increasing structure depth for the considered depth range. On the contrary, the increase of breaking force with structure depth in the case of CW micro – structuring is not clearly evidenced in this geometry, mainly due to higher values of standard deviation associated to the breaking force. The maximum breaking forces attainable are significantly higher in the case of ns micro – structuring, where the generated aspect ratio is higher.

Further investigation related to the joint interface characterization is needed to find the reasons that underlie the responsible mechanical interlock mechanisms for both studied geometries.

The achieved results evidence that an appropriate micro – structure can lead to high breaking forces for glass reinforced polyamide – steel joints.

Acknowledgements

The research leading to these results has received funding from the European Union's Seventh Framework Programme (FP7/2007-2013) under grant agreement 309993.

References

Paul, H., Luke, M., Henning, F., Evaluation of the Joining Mechanisms of Polymer Metal Components, Proceedings of ECC15 – 15th European Conference on Composite Materials. Venice, Italy, 1-7.

Grujicic, M., Sellapan, V., Omar, M. A., Seyr, N., Obieglo, A., Erdmann, M., Holzleitner, J., 2008. An Overview of the Polymer-to-Metal Direct-Adhesion Hybrid Technologies for Load-Bearing Automotive Components. Journal of Materials Processing Technology 197, 363-373.

Kawahito, Y., Tange, A., Kubota, S., Katayama, S., 2006. Development of Direct Laser Joining for Metal and Plastic, ICALEO Paper #604.

Katayama, S., Kawahito, Y., Niwa, Y., Kubota, S., 2007. Laser assisted Metal and Plastic Joining, Proceedings of the 5th Laser Assisted Net Shape Engineering, 41-51.

Bergmann, J.P., Stambke, M., 2012. Potential of Laser-Manufactured Polymer-Metal Hybrid Joints. Physics Procedia 39, 84-91.

Amend, P., Pfindel, S., Schmidt, M., 2013. Thermal joining of thermoplastic metal hybrids by means of mono- and polychromatic radiation. Physics Procedia 41, 98-105.

Hussein, F., Akman, E., Oztoprak, B., Gunes, M., Gundogdu, O., Kacar, E., Hajim, K.I., Demir, A., 2013. Evaluation of PMMA Joining to Stainless Steel 304 using Pulsed Nd:YAG. Optics and Laser Technology 49, 143-152.

Jung, K.W., Kawahito, Y., Takahashi, M., Katayama, S., 2013. Laser direct joining of carbon fiber reinforced plastic to zinc-coated steel. Materials and Design 47, 179-188

Roesner, A., Scheik, S., Olowinsky, A., Gillner, A., Poprawe, R., Schleser, M., Reisgen, U., 2011. Innovative Approach of Joining Hybrid Components. Journal of Laser Applications 23, 1-6.

Cenigaonaindia, A., Liebana, F., Lamikiz, A., Echegoyen, Z., 2012. Novel Strategies for Laser Joining of Polyamide and AISI 304. Physics Procedia 39, 92-99.

Georgiev, G.L., Baird, R.J., McCullen, E.F., Newaz, G., Auner, G., Patwa R., Herfurth, H., 2009. Chemical Bond Formation During Laser Bonding of Teflon® FEP and Titanium. Applied Surface Science 255, 7078-7083.

Wang, X., Li, P., Xu, Z., Song, X., Liu, H., 2010. Laser Transmission Joint between PET and Titanium for Biomedical Application. Journal of Material Processing Technology 210, 1767-1771.

Holtkamp, J., Roesner, A., Gillner, A., 2010. Advances in Hybrid Laser Joining. The International Journal of Advanced Manufacturing Technology 47, 923-930.

Fenech, H., Rohsenow, W.M., 1963. Prediction of Thermal Conductance of Metallic Surfaces in Contact. Journal of Heat Transfer 85, 15–24.

Yüncü, H., 2006. Thermal Contact Conductance of Nominally Flat Surfaces. Heat and Mass Transfer 43, 1-5.

Schenk, T., Richardson, I. M., Kraska, M., Ohnimus, S., 2009. Modeling Buckling Distortion of DP600 Overlap Joints due to Gas Metal Arc Welding and the Influence of the Mesh Density. Computational Materials Science 46, 977–986.